LRP 664/00 March 2000

Analysis of the dynamic response of the plasma in the presence of sawteeth on TCV

A. Manini, J.-M. Moret, I. Furno,
T.P. Goodman, M.A. Henderson

submitted for publication in
Plasma Phys. & Contr. Fusion

ISSN 0458-5895

ANALYSIS OF THE DYNAMIC RESPONSE OF THE PLASMA IN THE PRESENCE OF SAWTEETH ON TCV

A. Manini, J.-M. Moret, I. Furno, T. P. Goodman, M. A. Henderson

Centre de Recherches en Physique des Plasmas, Association EURATOM - Confédération Suisse, Ecole Polytechnique Fédérale de Lausanne, CH-1015 Lausanne EPFL, Switzerland

Abstract. Using the plasma temperature dynamic response to study heating deposition or transport mechanism is often precluded by coupling between the sawtooth instability and the power excitation, coupling which can even dominate the response. To diminish such a pollution of the signals, a method based on a Generalized Singular Value Decomposition technique has been tested. The dynamic response to ECH power excitations of the electron temperature inferred from soft X-ray emissivity has been studied for the experimental determination of the power deposition profile in the TCV tokamak. Experiments have been performed with square wave power modulation at 5 different frequencies. To test the effectiveness of the method, discharges with the ECH aiming at four different locations in the plasma have been performed as well as two series of discharges at low and high plasma current. It was possible to reduce the sawtooth contribution on average by a factor of 10. The Generalized Singular Value Decomposition has also been successfully used to treat the signals at the turn off of the ECH, with the purpose of developing a fast guess localization procedure to be applied after each discharge. A Harmonic Response Identification Method has been applied to determine the relative response of the plasma to the power perturbation. An accelerated tomographic inversion then recombines these elements in a radial amplitude and phase profiles of the response.

1. Introduction

Good knowledge of the Electron Cyclotron Heating (ECH) power deposition profile is essential for the experimental study of auxiliary heated plasmas (energy and particle transport, confinement, plasma stability), for profile tailoring, current drive, as well as for the verification of ECH ray tracing and absorption codes [1,2,3,4]. In TCV (Tokamak à Configuration Variable [5]) this is complicated by the combination of a large variety of plasma shapes (elongation $\kappa<2.58$, triangularity $-0.7<\delta<+1$, to date) and a versatile ECH launching system [6]. The dynamic response to ECH power excitation of the electron temperature inferred from soft X-ray emissivity is used in this paper to examine the ECH deposition. Both the hardware and the software of the 200 channel X-ray tomography diagnostic system of TCV are described in [7].

The experimental determination of the power deposition faces several problems, such as the need of avoiding the knowledge of transport mechanisms. Further complication is added by the coupling between the modulated ECH (MECH) and the sawtooth contribution to the soft X-ray emissivity. These problems have already been analyzed in other devices such as TCA [8], ASDEX [9] and RTP [10] and several different techniques have been adopted to circumvent the difficulties. The problems are reviewed in section 2.

The experimental set up and the discharge configurations adopted for the experiments presented in this paper are described in section 3.

The signals of the line integrated emissivity are first treated with a Generalized Singular Value Decomposition (GSVD [11]) in order to diminish the effect of the component due to the sawtooth instability; the signals are then analyzed with a Harmonic Response Identification Method (HRIM) and tomographically inverted to obtain the amplitude and phase profiles. This analysis procedure is fully described in section 4.

The results are presented in section 5. Particular weight is put on the sawteeth suppression, which can also be applied during other transients such as the turn on/off of the ECH.

Section 6 concludes with a brief summary and an outlook on future developments.

2. Problems

The experimental determination of the power deposition profile faces three main problems. First, it is well known that transport in hot magnetically confined plasmas is not yet understood [12]. Several aspects limit our present understanding: electron heat conduction across the magnetic field can exceed the neoclassical prediction by one to two orders of magnitude; degradation of confinement increases with input power; it is unsure whether transport is locally determined or if global parameters could determine transport throughout the system, so-called nonlocal effects [13,14]. Hence, we need to develop a method that provides the localization of the power deposition without the knowledge of heat diffusion and convection coefficients.

In TCV these basic questions are accompanied by the peculiarities of the device (see figure 1), which allows the production of a large variety of plasma shapes. In particular, one of the roles of TCV is the study of the influence of the plasma shape on confinement and energy and particle transport in ECH heated plasmas [15,16]. This large variety of shapes calls for a

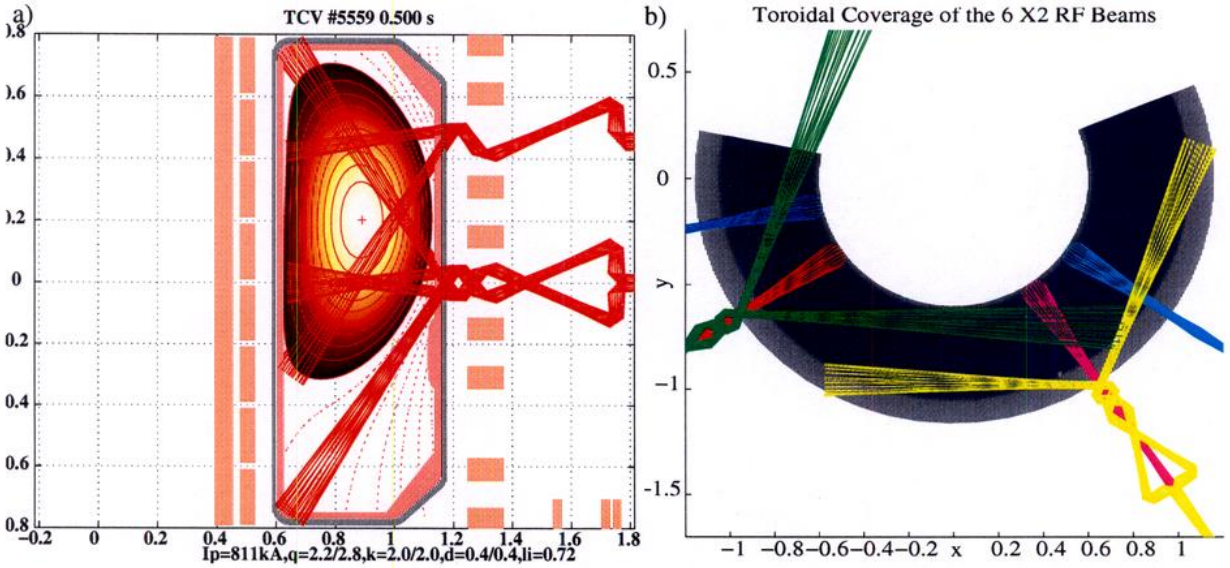

Figure 1. ECH launching system accessibility of TCV: (a) poloidal and (b) toroidal view. The launchers are located in the equatorial and upper lateral ports. Only the equatorial launcher has been used.

versatile ECH launching system, to aim the RF power at the plasma in all possible configurations. The ECH launching system will ultimately include 9 independent beams, 6 at the second harmonic (82.7GHz, 3MW total power) with independent poloidal and toroidal launching angles and 3 at the third harmonic (118GHz, 1.5MW total power) combined on one launcher with one independent poloidal launching angle. These particularities of the device, most specifically the shallow angle of incidence of the beam on the resonance and the possibility of aiming with large angles relative to the density gradients, imply that refraction effects of the EC waves could become important, and therefore a good knowledge of the electron density profile is required for correct power absorption prediction.

The method chosen for the purpose of power deposition localization is the study of the dynamic response of the electron temperature to modulated ECH. This technique forces us to take into account the third problem; namely, the mixing between the ECH induced modulation and the sawtooth activity of the plasma [10]. Figure 2 shows the case of an ECH heated plasma discharge performed with an ECH modulation frequency of ν_{mod} = 71.4 Hz. The peaks at the first and third harmonic of the modulation frequency are clearly visible, as well as

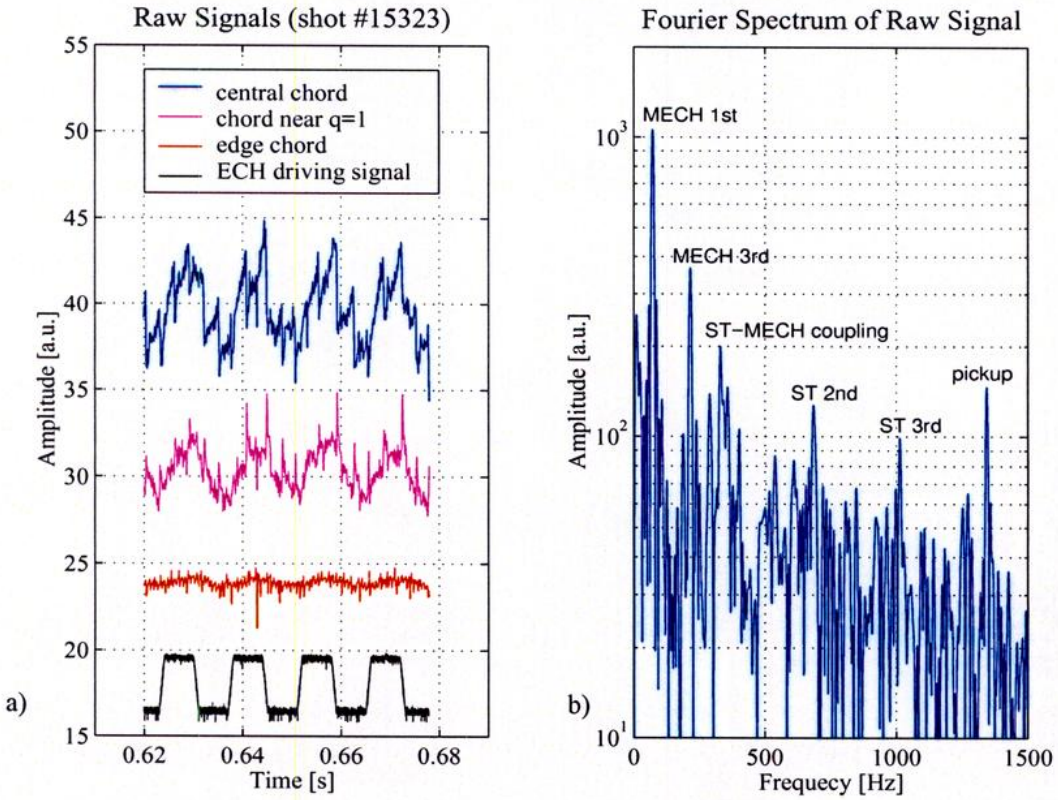

Figure 2. (a) Raw soft X-ray signals for different lines of sight. (b) Fourier spectrum of raw data: the different peaks related to different frequencies are visible, in particular the sawtooth-modulation coupling.

a wide frequency distribution around the main sawtooth frequency ($\nu_{ST} \sim 330$ Hz) with peaks at the main sawtooth frequency ν_{ST} and at $\nu_{ST} \pm \nu_{mod}$. This is a clear evidence of the presence of mixing between the modulation contribution and sawtooth activity.

An additional difficulty arises from the fact that the signals used are the soft X-ray emissivities. The X-ray emissivity depends not only on the electron temperature, but also on the electron density and on the effective charge of the plasma and is an integrated measurement.

3. Experimental set up

In a first step, in order to avoid complications due to the plasma shape dependence and the MHD activity produced by extreme shapes, which also limit the plasma current I_p to lower levels, the dynamic response of the plasma to ECH power perturbations has been measured in a relatively simple experimental scenario. A "typical" TCV plasma has been chosen with an elongation κ=1.6, a triangularity δ=0.3 and a line average density of ~1.5x10^{19}m^{-3}. A single gyrotron with a maximum power P_{max} = 500kW was used. The plasma configuration chosen

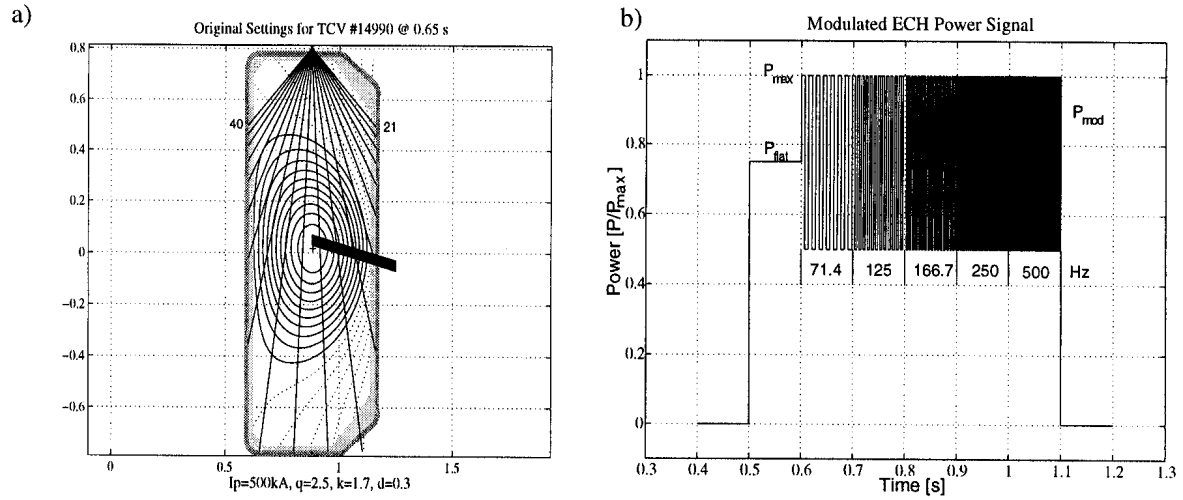

Figure 3. (a) ECH launching scenario for discharge #14990 (central deposition). The lines of sight of one camera at the top of the vessel are shown. For the different deposition locations the plasma was displaced vertically.(b) Modulated ECH power signal.

for the experiments requires the use of the equatorial launcher (see figure 3a) in order to heat the plasma with the smallest beam size and obtain a localized deposition.

To validate the signal processing technique used to suppress the sawtooth contribution, experiments were performed at low plasma current I_p=260kA, hence at relatively high safety factor q~4.5, and at high plasma current I_p=400kA (low safety factor q~2.5). As an illustration of the work that has been performed on all these discharges, a particularly extreme experiment performed at I_p=500kA will be used as example to show intermediate and final results of the elimination method.

For both current levels, different ECH deposition locations have been examined varying the vertical position of the plasma instead of the ECH poloidal launching angle to reduce the refraction effects mentioned earlier.

The dependence of the plasma response to different modulation frequencies has been investigated using square wave power modulation at all 5 frequencies (71.4, 125, 166.7, 250, 500Hz for 100ms) during each discharge. The intensity of the power modulation was $P_{mod} = \pm 1/3 \cdot P_{max}$ starting from a flat top level of $P_{flat} = 2/3 \cdot P_{max}$ (figure 3b).

4. Analysis procedure

The problem we are facing is the removal of the sawtooth oscillation from spatially resolved measurements in a self-consistent way, hence preserving transients that have a different physical origin, in our case the contribution to the signal due to the MECH. As previously seen in section 2, standard filtering of each measurement, using frequency elimination techniques, is not possible due to the strong mixing between sawtooth and MECH contributions. The idea in order to circumvent the problem, is to use the information stored in the relationship between the time evolution and the spatial structure imposed by the different transport mechanisms of the different dynamics. The time measurements can be seen as trajectories in a multi-dimensional space whose dimensions are the observation positions x. What we try to do is to find a technique constructing subspaces that allow the identification of the dynamics of interest, i.e. the trajectories of the sawteeth and of the MECH.

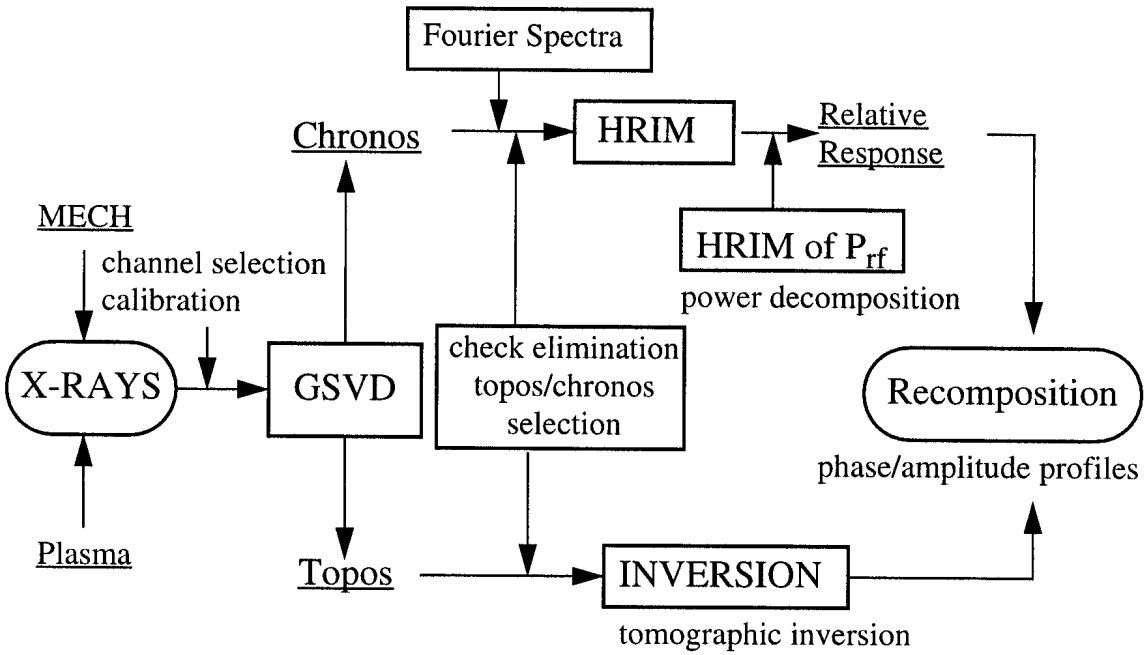

Figure 4. Procedure schematic.

Figure 4 shows an outline schematic of the analysis procedure. The signals whose lines-of-sight cross the plasma poloidal cross section are selected; because of the plasma-free regions of the vacuum vessel, not all lines-of-sight view the plasma. In order to separate the sawtooth activity from the power modulation contributions as well as the contribution due to pick-up noise caused by the coils of TCV, these signals are analyzed with two similar techniques called Singular Value Decomposition (SVD [7,17]) and Generalized Singular Value Decomposition (GSVD [11]) which will be presented in detail in sections 4.1.1 and 4.1.2. The two techniques decompose the signals providing a set of topos (spatial eigenvectors) and chronos (temporal eigenvectors). The topos and chronos relevant to the MECH are selected using the Fourier analysis of the chronos, which allows the identification of the frequency spectrum of the MECH. The selected topos are then submitted to a tomographic inversion, while the chronos are analyzed with the HRIM technique. A decomposition, using the same procedure as for the chronos, of the reference power signal (taken from the gyrotron cathode voltage) is used to determine the relative response at each harmonic. The relative responses and the inverted topos are then recombined to obtain the radial amplitude and phase profiles. Details of each step in the procedure are presented in the following sections.

4.1 The sawtooth suppression

4.1.1 The Singular Value Decomposition (SVD)

As a first attempt to diminish the sawtoothing contribution to the signals, the well known Singular Value Decomposition (SVD [7,17]) technique has been tested. The SVD tries to identify the spatial information of the dynamics of the system in constructing a new set of orthogonal basis vectors on which to project the trajectories. The main axes of this new basis are then supposed to coincide with the trajectories along which the dynamics evolve in space and time. Formally the spatio-temporal observables $u(x,t)$ are decomposed into a unique set of

orthonormal spatial and temporal modes

$$u(x,t) = \sum_{k=1}^{K} \alpha_k a^*_k(t) v_k(x) \tag{1}$$

with $\langle a^*_k a_l \rangle = \langle v^*_k v_l \rangle = \delta_{kl}$ ($\langle\ \rangle$ denotes scalar product); by convention the modes are ordered such that $\alpha_1 \geq \alpha_2 \geq \ldots \geq \alpha_K \geq 0$. If the observations are correlated in time and in space, then a few weights α_k usually dominate the expansion.

In practice, the SVD decomposes an $(M \times N)$ matrix X into three matrices U, S and V

$$X = U \bullet S \bullet V^{\dagger} \tag{2}$$

where the dagger † denotes the Hermitian adjoint. Both U and V are unitary, where U is an $(M \times M)$ and V an $(N \times N)$ matrix. The $(M \times N)$ matrix S is diagonal. If each row of X contains a time series of a physical quantity at a different location, the columns of U represent spatial eigenvectors, called topos, whereas the columns of V can be considered as temporal eigenvectors, called chronos. Due to the descending order of the singular values, X is decomposed into different components of descending relative importance.

Figure 5 shows the SVD analysis of the time traces of the line integrated soft X-ray emissivity of discharge #14990. The SVD has been performed in the time interval with a MECH at 71.4Hz. The first topos/chronos belong to the modulation contribution (but sawteeth are still clearly detectable) and the second ones belong to the sawtooth contribution (but MECH modulation is also still present). The third components belong to the pickup contribution. It is clearly visible that the sawtooth coupling between MECH (slow oscillation of column 2) and sawteeth (fast oscillation of column 2) is not separated from the modulation component itself with this method. Therefore, a more suitable method needs to be found.

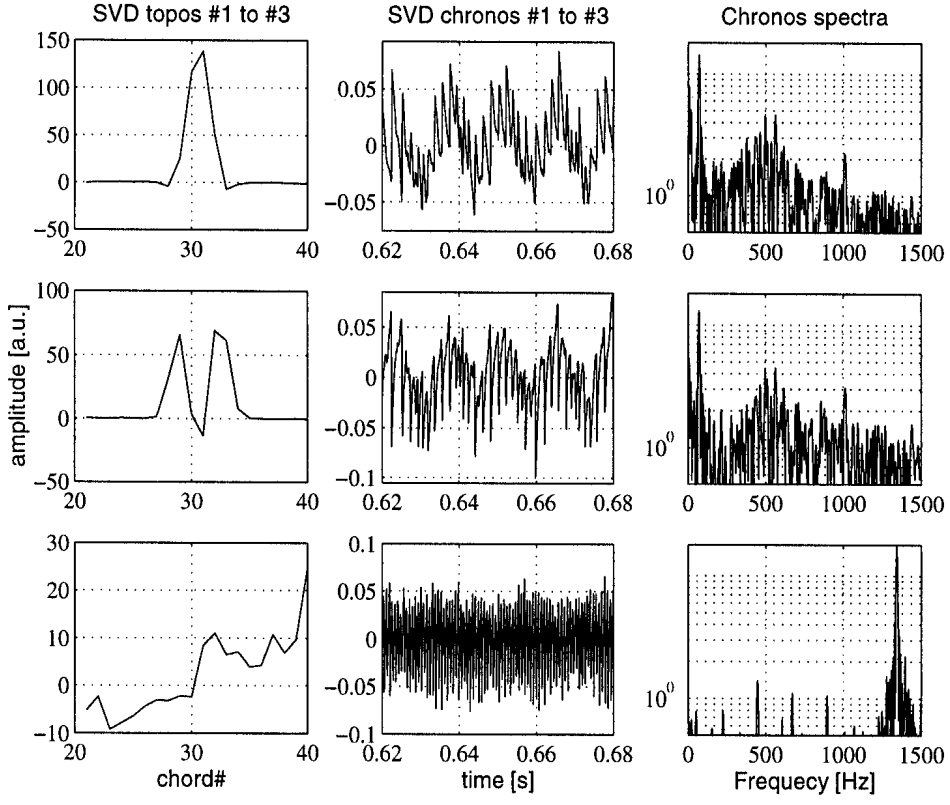

Figure 5. First three topos/chronos components of the SVD of discharge #14990.

4.1.2 The Generalized Singular Value Decomposition (GSVD)

4.1.2.1 Theory and optimization

The analysis with the GSVD is based on the same basic ideas of the SVD, but with a significant difference: it requires the possibility to make two different observations of the same system, one with only noise, in this case, the sawtooth activity, and one with the dynamic of interest. The main point of this technique is that it tries to identify the trajectories of the dynamic of the sawteeth in the first observation so that, once re-identified in the second observation, they can then be projected on the same basis and easily "removed". Resuming, the idea consists of finding a basis that enhances the representation of those trajectories we are interested in while "capturing" the least possible of the unwanted ones. Three assumptions need to be made:

1. The sawtooth oscillations and the transients generated by the MECH do not have the same spatial dynamics: they propagate differently and have different source terms.
2. The sawtooth oscillation is not strongly affected by the MECH in its propagation. The sawtooth amplitude and period may vary self-consistently, but not their propagation through the plasma.
3. The response to the power modulation is linear, which applies if the amplitude of the modulation component is much smaller than the average signal.

Let $u(x, t)$ denote the observations during the MECH and $y(x, t)$ the sawteeth dominated ones, that is, the plasma behavior without the MECH perturbation. The GSVD gives a common basis for $u(x, t)$ and $y(x, t)$ that optimizes the representation of the former while capturing the least possible of the latter. This basis is complete and unique, but not necessarily orthogonal

$$u(x, t) = \sum_{k=1}^{K} \alpha_k a^*_k(t) v_k(x) \tag{3a}$$

$$y(x, t) = \sum_{k=1}^{K} \beta_k b^*_k(t) v_k(x) \tag{3b}$$

The spatial modes $\{v_k(x)\}$, the topos, are not independent, in general $\langle v^*_k v_l \rangle \neq 0$ for $k \neq l$ ($\langle\ \rangle$ denotes scalar product). The temporal modes $\{a_k(t), b_k(t)\}$, the chronos, however, are orthonormal. By convention, the weights are normalized by $\alpha_k^2+\beta_k^2=1$. Figure 6 shows topos and chronos of the first five components given by the GSVD (also for discharge #14990). The first component is dominated by the modulation contribution and the other four contain only very small contributions, due to the sawteeth only, or to the coupling between sawteeth and MECH. One can also observe how the contribution due to the electric pickup is also considerably reduced.

Because of the normalization of the weights, the singular values α_k and β_k can be interpreted as cosines and sines of the separation angles between the two subspaces:

$$\theta_k = \operatorname{atan}\frac{\alpha_k}{\beta_k} \tag{4}$$

and the generalized singular eigenvalues $\sigma_k = \alpha_k/\beta_k$ as the signal to noise ratio

$$SSR_k = 20\log\frac{\alpha_k}{\beta_k} \tag{5}$$

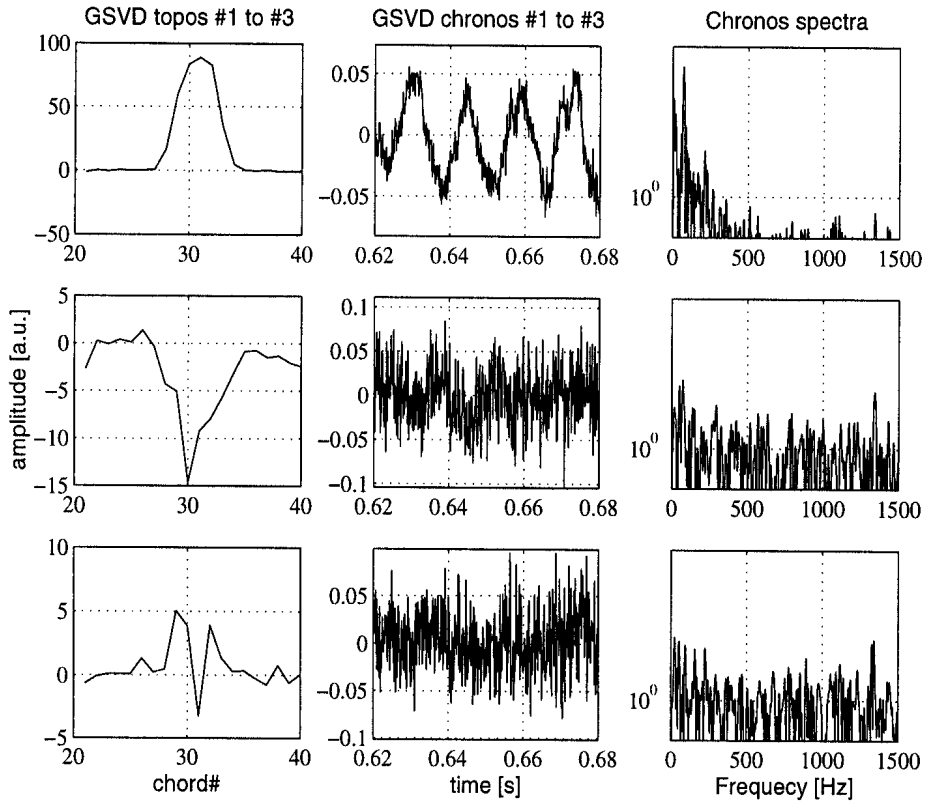

Figure 6. First three topos/chronos components of the GSVD of discharge #14990. The GSVD has been again performed in the time interval with a MECH at 71.4Hz. The first two topos/chronos belong to the modulation contribution (sawtooth contribution significantly reduced). The other contains mainly the noisy pickup.

The GSVD projects the trajectories on a new basis whose first axes preferentially capture $u(x, t)$ and conversely the last axes reveal $y(x, t)$ (if the generalized singular values are sorted in decreasing order). It is thus possible, truncating the expansion after a small number of components, to separate most of the dynamic of interest from the sawteeth contributions.
A good separation can be achieved with the basis vectors whose angular separation is either close to $\pi/2$ (signal with little noise) or close to 0 (noise with little signal). Angles around $\pi/4$ and signal-to-signal ratios near 0dB correspond to directions along which the separation is difficult. The faster the angular distribution drops from $\pi/2$ to 0, the better the separability [11].

Figure 7 shows the sawtooth reduction of the example discharge #14990. The main frequency components of the sawteeth are found at 500, 562, 430 and 465Hz. Comparison of their amplitude to the amplitude of the fundamental harmonic of the modulation at 71.4Hz shows a reduction, in the analyzed channel, of about a factor of 10. Studying discharge #15323, which was performed at a plasma current of 250kA (q~4.5), which means that the sawtooth contribution was already limited by the high q value, shows an average reduction of also a factor of 10. Tests in other situations show that the sawtooth components can be reduced by a factor of 10 in general.

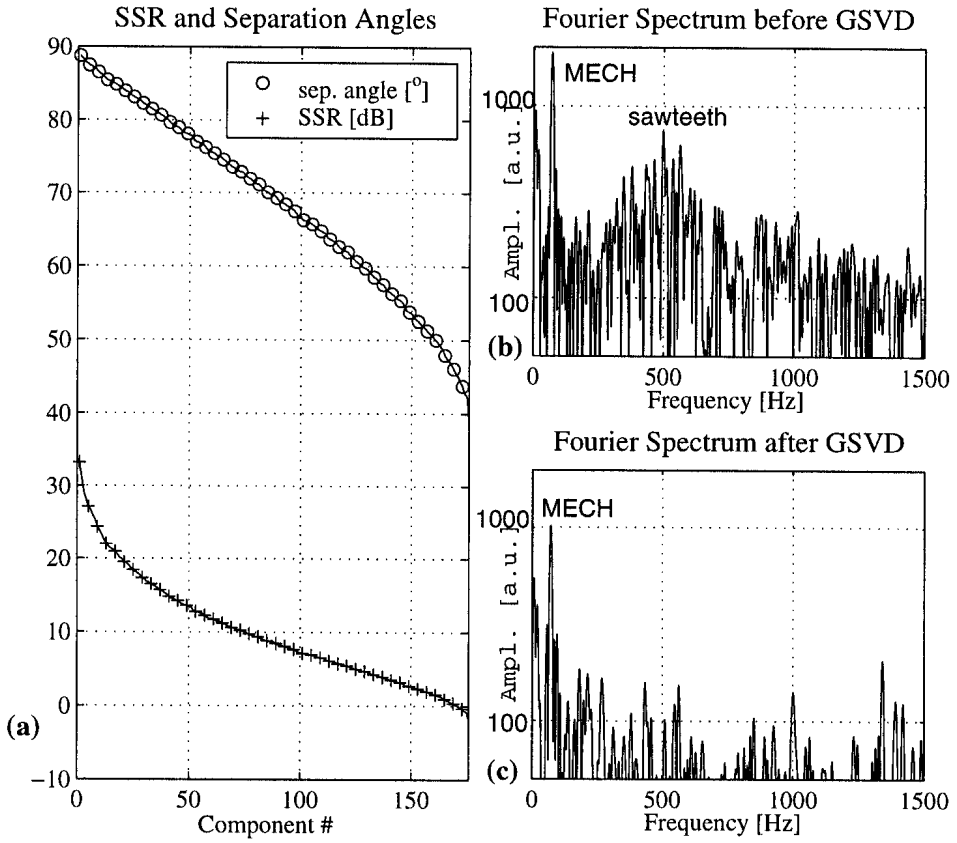

Figure 7. Example of good sawtooth elimination: shot #14990, selected first 4 components. (a) Signal-to-Signal Ratio of the components; (b) Fourier spectrum before the GSVD; (c) Fourier Spectrum after the GSVD.

4.1.2.2 Sawtooth reduction

In order to obtain the results displayed above, the procedure described had to be tested and optimized with respect to three important aspects: the normalizations chosen for u and y, the lengths of the time windows of u and y and the selection of the diodes to be used. The best separation has been found studying the behavior of separation angles θ_k and signal-to-signal ratios SSR_k as well as through Fourier analysis of the filtered signals. Best conditions were obtained with:

- a simple mean-subtraction normalization ($u_{norm} = u - \langle u \rangle$);
- the length of u being the whole modulation interval (100ms);
- the length of y containing 6 to 10 sawtooth periods (about 20ms);
- selecting all the diodes whose lines of sight cross the poloidal plasma cross section.

Figure 8 shows a summary of the sawtooth elimination analysis. Figure 8a shows the ratio between the sawtooth signal energy and the energy of the fundamental MECH harmonic before and after the GSVD at different frequencies. The value of the sawtooth energy has been averaged over chords 25 to 35 whose lines of sight are mainly concentrated towards the plasma center. While the ratio of the raw signals shows no variation with increasing MECH frequency, in the processed signals the ratio clearly shows a minimum in the frequency range between 100 and 200Hz, which means that the coupling between MECH and sawtooth contribution is better reduced with the modulation chosen in this interval. From the same figure it is also visible that the elimination naturally works better in the cases with q~4.5, in

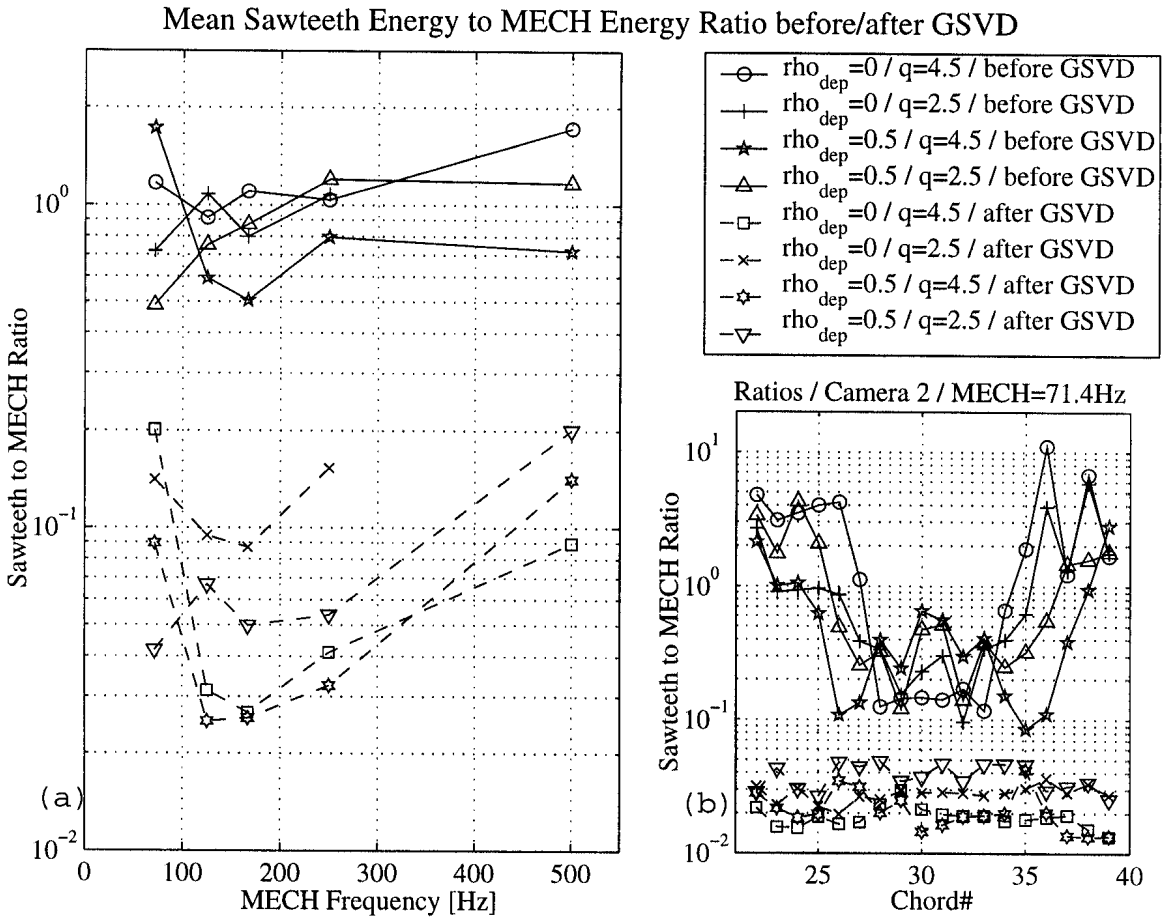

Figure 8. Sawteeth to MECH ratio. (a) Mean frequency dependence; (b) chord distribution of camera 2.

presence of small sawteeth. Figure 8b shows the spatial distribution of the ratio using the lines of sight of camera 2. The sawtooth contribution before the GSVD is clearly higher for the diodes whose lines of sight cross the plasma edge, while the ratio is reduced to a fairly constant average value after the reduction. It is also visible from the graph that, again, the GSVD works best for the plasmas with high safety factor. For plasmas of low q the method works best for central deposition.

Concluding this section, the GSVD has been tested and optimized and the sawtooth elimination has been applied and verified. The method allows a reduction of the sawtooth components by about a factor of 10, in the case of both small (q~4.5) or large (q~2.5) sawteeth.

4.2 The Harmonic Response Identification Method (HRIM) applied to the chronos

The electron temperature is composed of a modulation contribution superimposed on signals caused by changes in the main plasma parameters. The GSVD decomposes the signals providing a set of topos and their corresponding chronos. The time evolution of a certain part of the system is thus contained in the selected chronos. The idea of the HRIM is to simultaneously eliminate the base signal and to extract the complex amplitudes of the harmonics of the modulation frequency [18,19]. Mathematically this is expressed as

$$\hat{u}(t) = \left[\sum_{n=1}^{N} Re(U_n)\cos(n\omega t) + Im(U_n)\sin(n\omega t) \right] + \langle u \rangle + \frac{d\langle u \rangle}{dt}(t - t_0) \qquad (6)$$

We do the same for the EC power signal, which is used as the reference

$$\hat{p}(t) = \left[\sum_{n=1}^{N} Re(P_n)\cos(n\omega t) + Im(P_n)\sin(n\omega t) \right] + \langle p \rangle + \frac{d\langle p \rangle}{dt}(t - t_0) \tag{7}$$

U and P are the modulation complex amplitudes of the X-ray signals u and reference power signals p, $\hat{u}$ and $\hat{p}$ the reconstructed signals with the HRIM. We can then calculate the complex relative response of each harmonic (n odd in the presence of square modulation)

$$A_n = \frac{U_n}{P_n} \tag{8}$$

Equations (6) and (7) can be considered as simple vector-matrix multiplications and can be easily solved numerically.

4.3 The tomographic inversion of the topos

The soft X-ray data used for the analysis are signals integrated along the lines of sight of the detectors. In order to gain information on their radial profiles, it is necessary to perform a tomographic inversion. Soft X-ray tomography in TCV is described in detail in [7]. A classical inversion would require one inversion for each time point of the selected interval, which in our case would consist of at least 1000 inversions. The GSVD allows a reduction of this number to only a few inversions since only the selected topos need to be inverted. The inverted topos will be then recomposed with each harmonic of the relative response obtained with the HRIM procedure, resulting in amplitude and phase profiles for several harmonics of the modulation frequency.

Mathematically, the tomography problem consists of solving the system of integral equations

$$f_l = \int_{S_l} g\,ds \tag{9}$$

f_l denotes the line integrated data, g the emissivity distribution and the integral is performed on a cone along the lines of sight. The tomography problem is solved using a pixel method [7]. One advantage of this method is that no explicit reference is made to the flux surface geometry, the second advantage is the straightforward way the system of integral equations (9) is transformed to a system of algebraic equations: we store the $n_{pixel} = n_x \cdot n_y$ values g_i of our two-dimensional emissivity distribution as lines of a column vector g. The n_l line integrated data f_l form a column vector f. We obtain

$$f = \hat{T} \bullet g \tag{10}$$

A direct inversion of $\hat{T}$ is almost always impossible (many fewer lines of sight than pixels). Since we always work in the limit of many fewer equations (hence f_l's) than unknown g_i's, to obtain a unique solution, we look for a minimum of a functional ϕ, which may be written as

$$\phi = \frac{1}{2}\chi^2 + \alpha R \tag{11}$$

R is a regularizing functional, α a parameter determining the weighting between the statistical goodness of the fit (represented by χ^2), and the requirements imposed on g by R (for example smoothness). Different choices of R can be made. For our purposes, a method relying on the Fisher information has been chosen.

The minimum Fisher method for the inversion requires the data to be inverted to be positive definite. This is not necessarily the case for the topos obtained with the GSVD, we need therefore to slightly modify the data to circumvent this problem. Let us define:

$\langle u \rangle$: amplitude of the mean signal
u_k : the topos of the GSVD
$\Im$: the operator performing the inversion

Since the amplitude of the topos u_k is much smaller than the amplitude of the mean signals $\langle u \rangle$ (linear response), we can consider them as small perturbations of $\langle u \rangle$. We can then make the inversions

$$\hat{e} = \Im(\langle u \rangle)$$

$$\hat{e}^*_k = \Im(\langle u \rangle + u_k)$$

The inverted topos can then be calculated with the simple subtraction

$$\hat{e}_k = \hat{e}^*_k - \hat{e}$$

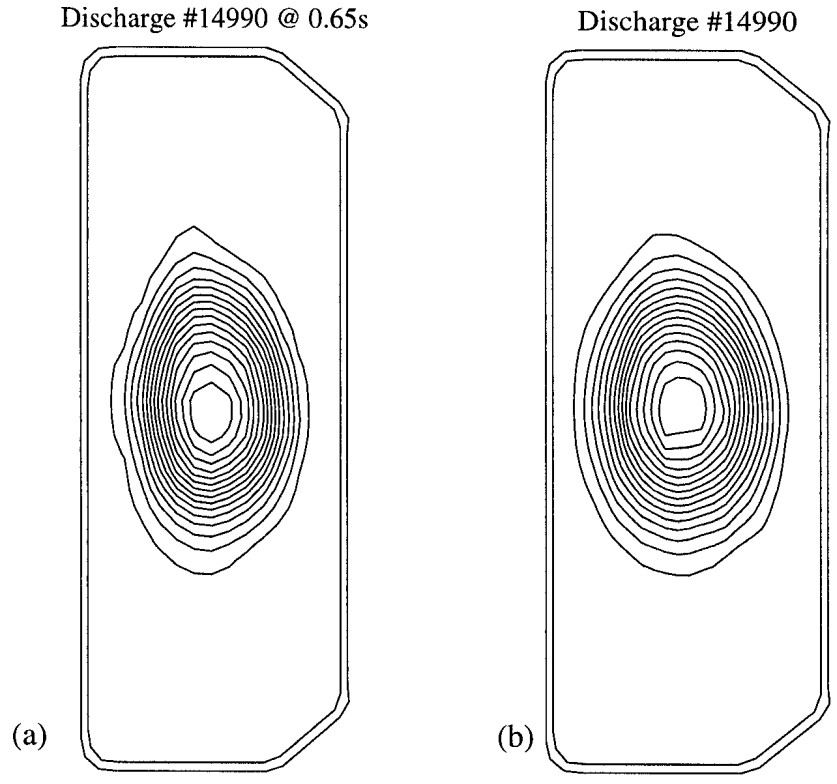

Figure 9. Comparison of full tomographic inversion (a) and inversion of first GSVD topos (b).

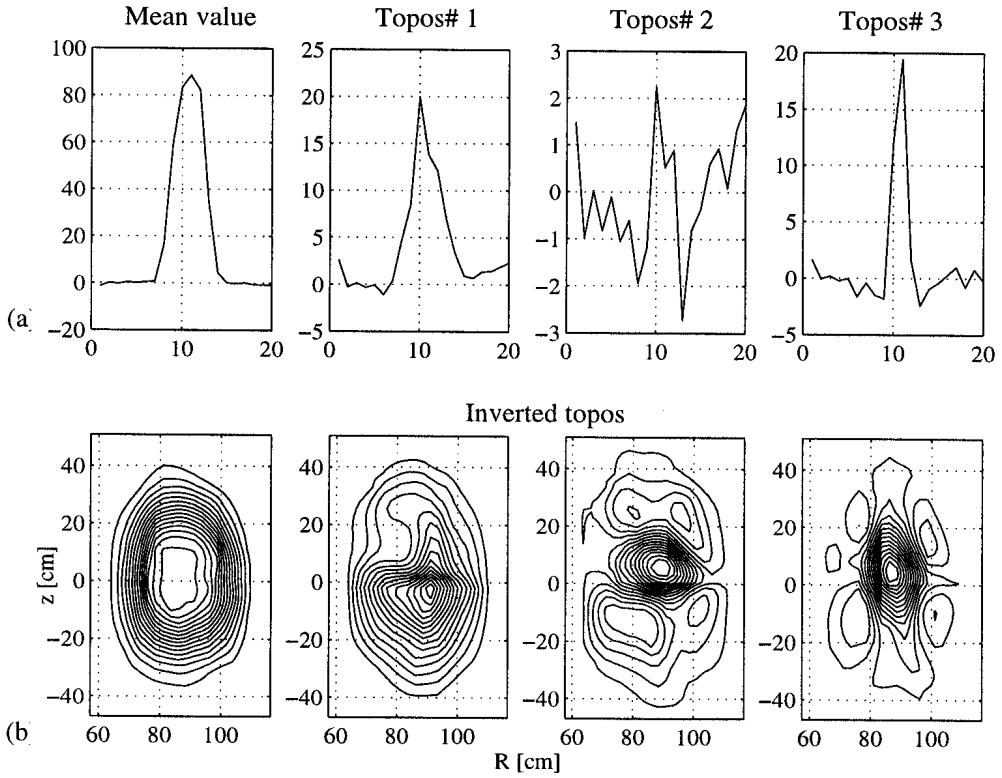

Figure 10. First 4 topos before (a) and after (b) the tomographic inversion (shot# 14990).

Comparison between "classical" inversion and "limited" inversion shows good agreement in the reconstruction of the emissivity distributions (see figure 9). The inverted topos are then recomposed with the relative responses to obtain amplitude and phase profiles for the chosen harmonics of the power modulation frequency.
10a the main mode m=0 (second from the left) related to the MECH perturbation is clearly detectable (the first curve represents the mean value of the signals for camera 2). Figure 10b shows the tomographically inverted topos on the two dimensional grid.

Concluding this subsection, the GSVD allows a reduction of the number of required inversions to a very limited number (3 to 6), as opposed to the classical method which requires one inversion per time step.

5. Results

The above described procedure has been applied to a series of experiments planed for testing its effectiveness for different power deposition in the plasma. The plasma dynamic response was in particular studied at the shut off of the ECH and during the modulation phases. The figures below show the results obtained.

Figure 11 shows an example of a fast method for a rough determination of the ECH deposition profile from the plasma evolution at the shut off of the ECH. Most of the time, this procedure cannot be applied in a straightforward way, because the shut off often coincides with a sawtooth crash. The GSVD allows the "elimination" of the crash in order to have a reliable and clean signal without sawtooth contributions. The figure shows in particular the case of discharge #15324, which was performed with the ECH aiming at about 0.5 normalized radius. The gyrotron was aiming at the region R = 85cm, z = 0cm, which corresponds to the

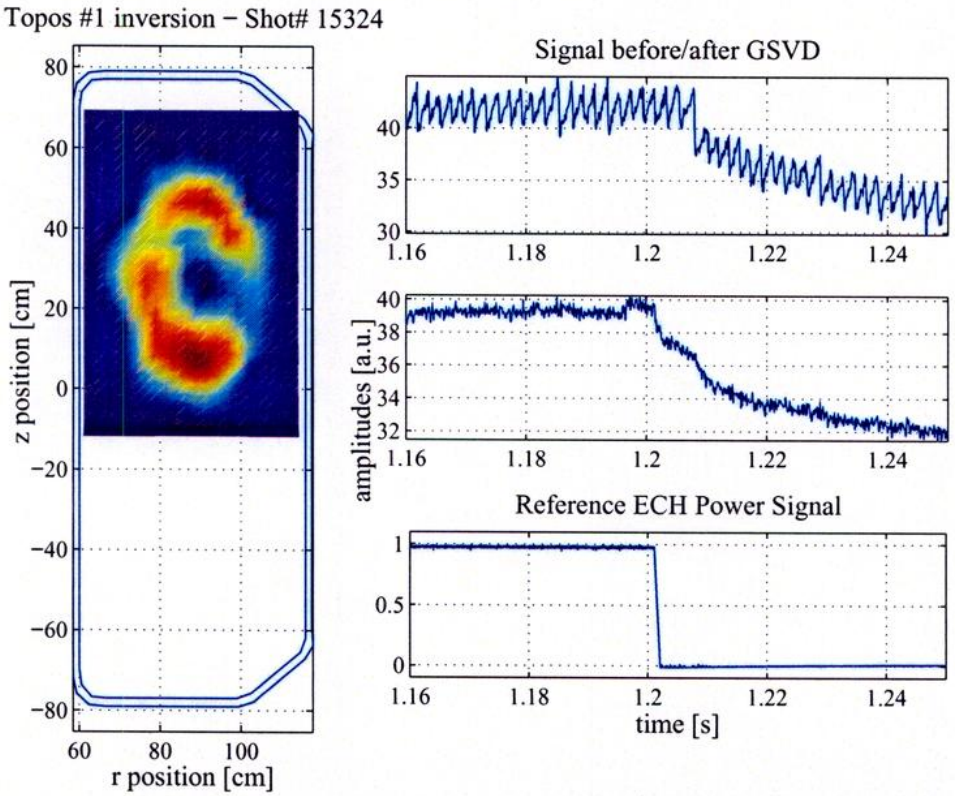

Figure 11. ECH shut off analysis of discharge# 15324. On the left, the inverted topos #1 shows what is probably the ring of the power deposition. On the right, the signal before and after the reconstruction with the GSVD and the ECH reference power signal.

location of the ring of higher emissivity obtained from the inversion of the first topos of the GSVD.

Figure 12 shows the comparison in the results for three different power depositions. The three shown discharges were performed at high plasma current (I_p = 400kA). The deposition location was displaced varying the plasma vertical position. The figure shows the estimated

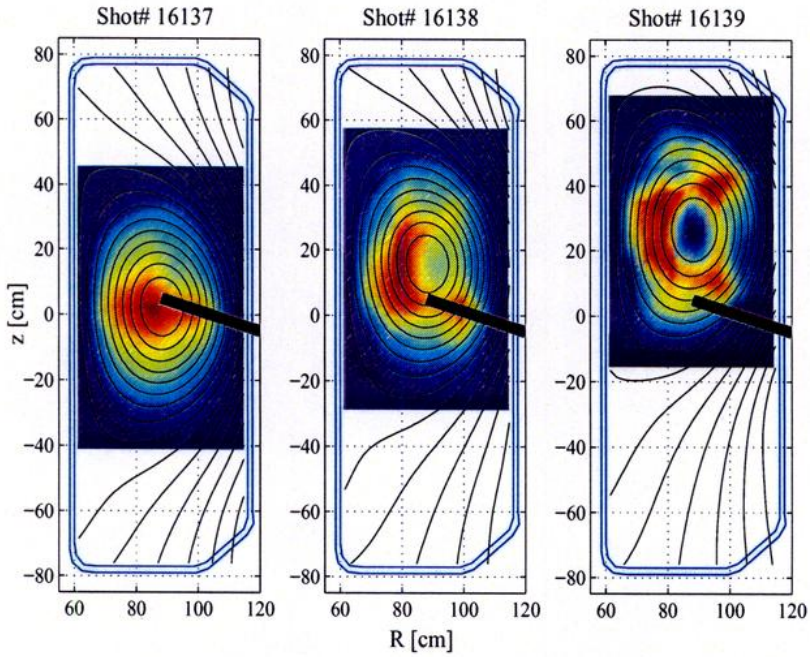

Figure 12. Tomographic inversion of topos# 1 for discharges with ECH aiming at three different locations.

ECH wave trajectory and the inverted emissivity distribution related to the shut off of the heating. The displacement of the maximum of the amplitude of the emissivity follows the displacement of the ECH power deposition.

It is clear that this method gives only a rough estimation of the deposition localization, but, thanks to the small number of calculations needed to get the result, it can be useful during ECH experiments, because it allows a fast check of the experimental set up. This is particularly important for TCV, because of its large variety of possible plasma shapes and because of the versatility of the ECH launching system.

Figure 13 shows the case where best results were obtained for the calculation of the

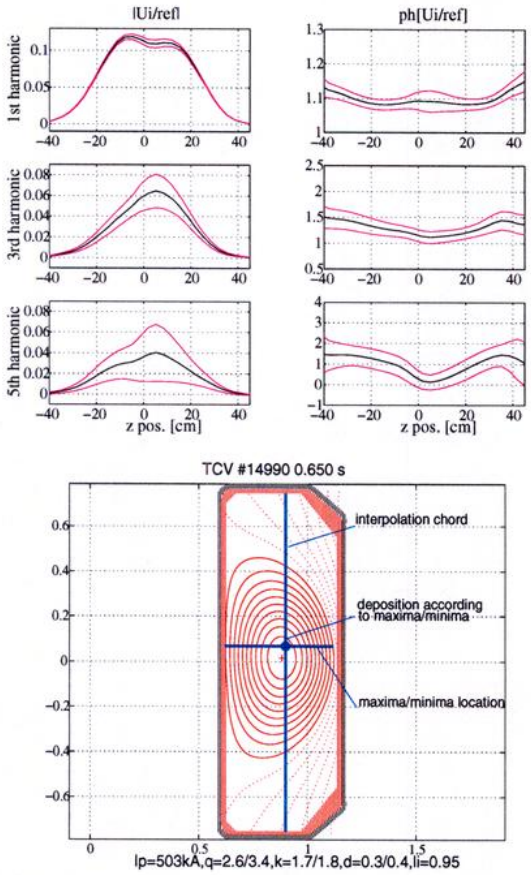

Figure 13. Amplitude and phase profiles of the plasma response for discharge #14990, for which best agreement was found between the ECH aiming settings and the amplitude and phase profiles.

amplitude and phase profiles during the MECH, the case in which good agreement was found between the ECH aiming settings expectations (central deposition) and the location of the maxima and minima in the amplitude and phase profiles.

6. Discussion and conclusions

The first problem arises from the fact that the whole analysis is performed using the line integrated soft X-ray emissivity signals. The soft X-ray emissivity has the intrinsic disadvantage of being strongly dependent also on the electron density and on the effective charge of the plasma. For the electron density in particular, it has been observed [20] that it reacts in opposite phase as the MECH and that it is also subject to recycling due to the particles exhaust from the internal wall of the vacuum vessel whom, in TCV, is almost entirely covered by carbon tiles. This means that, if the soft X-ray emissivity has to be used for the analysis of the data, the electron density response to the MECH also needs to be considered and understood, a task which is not necessarily straightforward.

Another problem related to the soft X-rays is due to the fact that they are integrated signals, which means that, in order to obtain local emissivities, a tomographic inversion of the data is also needed. All the problems related to the soft X-rays will be circumvented in future experiments with the installation of an ECE diagnostic system for a direct measurement of the local electron temperature.

Concluding, the soft X-ray emission of the plasma of TCV in the presence of MECH has been investigated in order to analyze the dynamic response of the plasma in the presence of sawteeth. Suppression of the coupling between the contributions in the X-ray intensity from the sawtooth instability and the MECH has been achieved using the GSVD method which was optimized by choosing a mean-subtraction normalization. The quality of the separation was found to depend on the choice of discharge time windows used in the analysis, the diode viewing chords and the modulation frequency. The sawtooth contribution could be reduced by a factor of 10 in most cases. A frequency dependence study has shown that the sawtooth reduction is more effective for modulation frequencies between 100 and 200Hz. Deeper studies are needed in order to "define" an allowable upper limit for the amplitude of the sawtooth contribution to the signals.

The HRIM has been successfully used in the frequency decomposition of the selected chronos and has been verified to correctly reconstruct the chronos themselves.

The spatial emissivity distribution was shown to be well reconstructed with a tomographic inversion of a limited number of topos terms. In particular, adapting the procedure to the shut off of the ECH it was possible to analyze the plasma response and to calculate a rough deposition profile inverting only the first topo of the GSVD.

Acknowledgements

Particular thanks to the TCV team, without whom this work would not be possible.
This work was partly supported by the Swiss National Science Foundation.

References

[1] V. F. Andreev *et al*, *Nuclear Fusion*, **33** (1993) 499
[2] U. Gasparino et al, *Plasma Phys. Control. Fusion*, **40** (1998) 233
[3] M. Cox *and* D C Robinson, *Plasma Phys. Control. Fusion*, **30** (1988) 1431
[4] G. M. D. Hogeweij *et al*, *Plasma Phys. Control. Fusion*, **34** (1992) 641
[5] F. Hofmann *et al*, *Plasma Phys. Control. Fusion*, **36** (1994) B277
[6] M. A. Henderson *et al*, *4th Int. Workshop Microw. in Plasmas*, LRP 643/99 (1999)
[7] M. Anton *et al*, *Plasma Phys. Control. Fusion*, **38** (1996) 1849
[8] J.-M. Moret *et al*, *Nuclear Fusion*, **33** (1993) 1185

[9] F. X. Söldner *et al*, *Phys. Review Letters*, **57** (1986) 1137
[10] A. Jacchia *et al*, *Nuclear Fusion*, **34** (1994) 1629
[11] T. Dudok de Wit *et al*, *Phys. Plasmas*, **5** (1998) 1360
[12] N. J. Lopes Cardozo, *Plasma Phys. Control. Fusion*, **37** (1995) 799
[13] A. Jacchia *et al*, *Phys. Plasmas*, **2** (1995) 4589
[14] K. W. Gentle *et al*, *Phys. Review Letters*, **74** (1995) 3620
[15] J.-M. Moret *at al*, *Phys. Review Letters*, **79** (1997) 2057
[16] H. Weisen *et al*, *Plasma Phys. Control. Fusion*, **37** (1997) 1741
[17] W. H. Press *et al* 1992, *Numerical Recipes in FORTRAN: The Art of Scientific Computing*, 2nd edn (Cambridge: Cambridge University Press)
[18] J.-M. Moret *et al*, *Nuclear Fusion*, **32** (1992) 1241
[19] J.-M. Moret, *thesis no. 758 of the EPF Lausanne*, LRP 358/88 (1988)
[20] I. Furno *et al*, *Proc. 26th EPS Conf. on Control. Fusion and Plasma Physics* (1999)